Effect of Land-Cover Type on the SMAP Active/Passive Soil Moisture Downscaling Algorithm Performance

Xiaoling Wu, Jeffrey P. Walker, Christoph Rüdiger, and Rocco Panciera

***Abstract*—A brightness temperature (Tb) downscaling algorithm based on the synergy between active and passive microwave observations is tested using airborne data that simulate the Soil Moisture Active Passive (SMAP) mission of the National Aeronautics and Space Administration scheduled for launch in January 2015. While this algorithm has been adopted as the baseline for SMAP, it has only been tested on a limited variety of land uses and vegetation types. Consequently, this study evaluates the SMAP active/passive downscaling algorithm using data with varied conditions. The SMAP experiment conducted in Australia has been used for this purpose. The algorithm was applied over several 9 km $\times$ 9 km pixels with different land covers, so as to evaluate the accuracy of this algorithm under different heterogeneity levels. Brightness temperatures were downscaled from 9 to 3 km (approximating the resolution ratio of SMAP downscaling approach) across nine days of data. Results show that the root-mean-square error of Tb in grassland could meet the 2.4-K target accuracy of SMAP, while in cropping, it was 2 K higher than the target. The influence from water bodies was also assessed and confirmed to have a significant impact if not removed prior to downscaling.**

***Index Terms*—Backscatter, brightness temperature, downscaling algorithm, Soil Moisture Active Passive (SMAP), Soil Moisture Active Passive Experiment (SMAPEx).**

I. Introduction

SURFACE soil moisture is the key to global water cycle monitoring, weather forecasting, prediction of drought and flood, and modeling of evaporation [1]–[4]. In particular, soil moisture plays an important role in the interaction between the land and the atmosphere, as it determines the distribution of energy at the subsurface, consequently impacting the associated water fluxes. With the development of remote sensing technology, soil moisture measurement at the global scale has become more economically feasible than traditional *in situ* station measurement [5]. However, there remain challenges associated with spatial resolutions.

Manuscript received May 19, 2014; revised September 2, 2014; accepted October 2, 2014.

X. Wu, J. P. Walker, and C. Rüdiger are with the Department of Civil Engineering, Monash University, Clayton, Vic. 3800, Australia (e-mail: xiaoling.wu@monash.edu; jeff.walker@monash.edu; chris.rudiger@monash.edu).

R. Panciera is with the Cooperative Research Centre for Spatial Information, The University of Melbourne, Melbourne, Vic. 3053, Australia (e-mail: pancerarocco@gmail.com).

Color versions of one or more of the figures in this paper are available online at http://ieeexplore.ieee.org.

Digital Object Identifier 10.1109/LGRS.2014.2364049

The European Space Agency launched the Soil Moisture and Ocean Salinity (SMOS) satellite in 2009, as the first-ever soil-moisture-dedicated satellite using passive microwave remote sensing technology [6]. Compared to other remote sensing techniques such as optical sensors, which are substantially impacted by atmospheric conditions and vegetation, microwave remote sensing has a more direct connection with surface soil moisture. Moreover, the vegetation and atmosphere are relatively transparent at lower frequencies, making it the more promising approach for soil moisture mapping [7]. However, at L-band, the preferred frequency for soil moisture mapping, the spatial resolution achieved from currently feasible passive microwave satellite configurations is on the order of $\sim$40 km, resulting in limitations on hydrometeorological applications such as regional weather forecasting, flood prediction, and agricultural activities that have a resolution requirement of better than 10 km [8], [9]. Although active microwave remote sensing provides a much higher spatial resolution ($\sim$3 km), it is less sensitive to changes in soil moisture due to the confounding effects of vegetation and surface roughness. Consequently, the National Aeronautics and Space Administration has developed the Soil Moisture Active Passive (SMAP) mission [10] scheduled for launch in January 2015, which will merge passive and active observations and thereby overcome their individual limitations, thus providing a soil moisture product with resolution better than 10 km at a target accuracy of 0.04 m^3/m^3.

Several downscaling methods have been proposed that use the synergy between passive and active data, such as the Bayesian merging method [11] and change detection method [12], [13]. However, the algorithm tested in this study is the baseline algorithm adopted by the SMAP mission [14]. This algorithm is based on the linear relationship between passive and active observations, which has been tested mostly using synthetic data and a limited number of suitable experimental data sets mostly in the U.S. [14], [15]. This baseline algorithm for SMAP was recently studied by Wu *et al.* [16] using airborne observations from the Soil Moisture Active Passive Experiment (SMAPEx) [17] in Australia. This was by necessity applied to a single SMAP-radiometer-sized site without differentiating the land-cover types across the entire site. That study was found to yield mediocre results, believed to be due to the diversity in land cover. Thus, a more extensive assessment of this baseline algorithm over a variety of land-cover types is required, in order to investigate the influence of different land covers on the resulting downscaling performance.

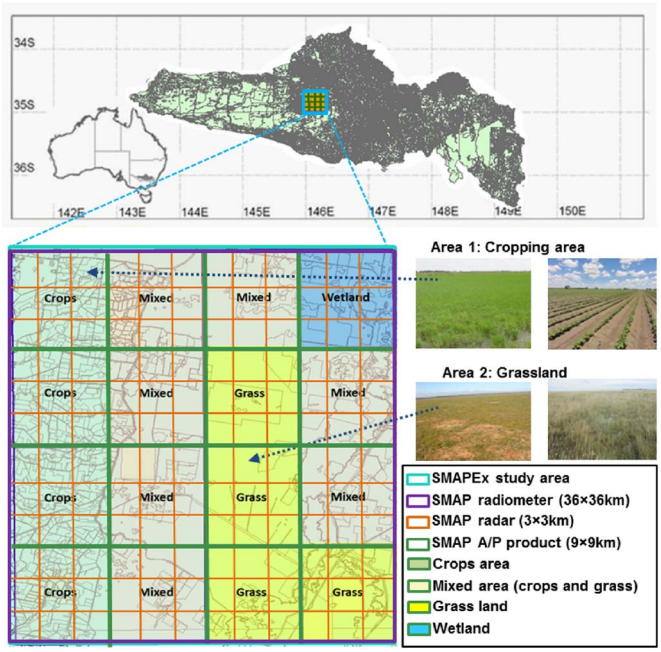

Fig. 1. Overview of the SMAPEx site showing the SMAP-sized-radiometer-pixel study area (approximately 36 km × 36 km) and the sixteen 9 km × 9 km areas used in this study, classified according to four dominant land-cover types (crop, grassland, mixed crop/grassland, and wetland).

The SMAPEx study area is composed of land covers including irrigated and nonirrigated cropping fields, grasslands, small forests, riverside trees, and some water bodies. Rather than applying the downscaling algorithm to the entire area as a single SMAP pixel [16], the objectives of this study were as follows: 1) to evaluate the accuracy of the SMAP baseline algorithm with respect to different land-cover types by dividing the entire SMAPEx site into distinct 9-km subregions according to the dominant land cover and 2) to assess the assumed linear relationship between brightness temperature (Tb) and backscatter (σ) and how it varies with land-cover type. Understanding the influence of surface heterogeneity on the resulting downscaling performance is important for its application to the forthcoming SMAP mission at global scale.

II. Data Set

The SMAPEx field site was chosen for testing the SMAP algorithm performance due to its flat topography, widely distributed monitoring stations, and spatial variability in soil, vegetation, and land use [17]. The SMAPEx site in Fig. 1, with location at $-34.67°$ N to $-35.01°$ N and $145.97°$ E to $146.36°$ E, has SMAP simulated data from airborne observations across a SMAP-sized radiometer pixel of around 36 km × 38 km. This pixel exhibits a landscape typical of southeastern Australia.

Data were collected using an airborne simulator, a platform providing active/passive microwave observations at high spatial resolution at L-band frequency, with polarizations (pols) and repeat interval similar to SMAP. The facility includes the Polarimetric L-band Multibeam Radiometer (PLMR) and the Polarimetric L-band Imaging Synthetic aperture radar (PLIS), providing 1-km Tb and 10-m σ when flown at 3000-m altitude. After being normalized for incidence angle to $40°$ viewing angle and aggregated to the appropriate spatial resolutions [18], the data may be used for development and testing of algorithms applicable to SMAP viewing configuration. The data used in this study were from the third field campaign (SMAPEx-3), which was conducted during September 5–23, 2011. The main flights provided a nine-day time series of SMAP-like observations with a two–three-day revisit time over a 36 km × 38 km area, equivalent to one pixel of the SMAP Equal Area Scalable Earth (EASE) grid at $35°$ S latitude; for application in this study, data were processed to 1-, 3-, and 9-km spatial resolutions for Tb and 1-km spatial resolution for σ.

Full details of the airborne data processing to match SMAP observations are given by Wu *et al.* [18], so only the details pertinent to this study are reported here. The airborne data were incidence angle normalized to the $40°$ of SMAP using a cumulative-distribution-function-based method [19], with an estimated error of approximately 2.5 K for PLMR at 1-km resolution and 0.8 dB for PLIS at 1-km resolution. These errors are comparable to those expected for SMAP, being approximately 1.0 dB for σ at 3-km resolution and 1.3 K for Tb at 36-km resolution. Whereas, in the case of SMAP, the 36-km-resolution Tb will be downscaled to 9 km using 3-km σ, in this study, 9-km-resolution Tb pixels aggregated from the original 1-km PLMR data are downscaled to 3 km using 1-km σ. The reason for choosing 9-km focus areas with 9-km Tb and 1-km σ was to test the downscaling algorithm over a larger variety of land cover than that possible when considering the whole SMAPEx site as a single SMAP pixel, as done in [16]. Moreover, the choice of 3 km as the final downscaling resolution was to maintain a similar resolution ratio between Tb and σ and the downscaled product, i.e., approximately $9:1:3$, as for SMAP. By distinguishing the land-cover type of each 9 km × 9 km pixel, this study provides a more in-depth testing of the baseline downscaling algorithm while also providing performance statistics of the baseline downscaling algorithm with respect to the different land covers of each 9-km pixel.

The various 9 km × 9 km areas and their dominant land-cover type are shown in Fig. 1, whereby: 1) four pixels mostly occupied by crops (a mix of bare soil, barley, and wheat at intermediate growth stage and mature canola fields); 2) four pixels with grasslands; 3) seven pixels with mixed land-cover types, approximately 50% crop and 50% grassland; and 4) one pixel with a 5-km^2-sized water body, termed here as "wetland." Before implementation of this algorithm, water bodies were removed in all pixels except the wetland pixel, so as to analyze the downscaling performance according to different land-cover types but without the influence from water bodies. In addition, inclusion of the wetland allows the water-body impact on the downscaling accuracy to be investigated.

III. Downscaling Algorithm

The baseline downscaling algorithm to be implemented by SMAP is based on the assumption of a near-linear relationship between Tb and σ. The following naming convention of "C" (coarse) and "F" (fine) represents the PLMR Tb (9 km) and PLIS σ (1 km), respectively. The algorithm is briefly described

here, with full details available in [14]. Implementation of this method requires a background Tb at C resolution, with the variation of Tb imposed by the distribution of fine-scale σ within C modulated by $\beta(C)$ of the linear regression between Tb and σ at C resolution according to

$$\mathrm{Tb}_p(F_j) = \mathrm{Tb}_p(C) + \beta(C) \times \{[\sigma_{pp}(F_j) - \sigma_{pp}(C)] + \Gamma \times [\sigma_{pq}(C) - \sigma_{pq}(F_j)]\} \quad (1)$$

where p indicates h-pol and v-pol and pp means co-pol of radar observations, including hh-pol or vv-pol. $\mathrm{Tb}_p(F_j)$ is the brightness temperature of pixel "j" of resolution F, and $\sigma_{pp}(F_j)$ is the radar backscatter of pixel "j." In this letter, the value for $\sigma_{pp}(C)$ was obtained by aggregating 10-m-resolution PLIS data within the coarse footprint C, with $\mathrm{Tb}_p(C)$ aggregated from 1-km PLMR observations. Consequently, $\beta(C)$, which depends on land-cover type as well as surface roughness, is assumed to be time invariant and homogeneous over the entire pixel, and it can be obtained through the time series of $\mathrm{Tb}_p(C)$ and $\sigma_{pp}(C)$. Since the radar also provides high-resolution hv-pol backscatter measurements at resolution F, which are mainly sensitive to vegetation and surface roughness, the subgrid heterogeneity of vegetation/surface within resolution C can be captured as $[\sigma_{pq}(C) - \sigma_{pq}(F_j)]$ by the radar, where pq represents hv-pol. This heterogeneity indicator is then converted to variations in co-pol backscatter by multiplying a sensitivity parameter Γ for each particular grid cell C and season defined as $\Gamma = [\delta\sigma_{pp}(F_j)/\delta\sigma_{pq}(F_j)]_C$. The term $\Gamma \times [\sigma_{pq}(C) - \sigma_{pq}(F_j)]$ can be described as the projection of the cross-pol subgrid heterogeneity onto the co-pol space, thus converting the information of vegetation and surface characteristics to the variation of co-pol backscatter. This term is converted to Tb through multiplication by $\beta(C)$ in (1). Using (1), downscaled Tb at 3-km resolution can be obtained in two ways: 1) by aggregating the downscaled 1-km-resolution Tb to 3-km resolution and 2) by directly downscaling to 3-km resolution. According to the study by Wu *et al.* [16], the two methods provide very similar results. In addition, Wu *et al.* [16] showed that σ at vv-pol has a better correlation with Tb than σ at hh-pol, and therefore, σ at vv-pol was used in this study to estimate β and applied to (1).

IV. Results

A. Estimation of β and Γ

The robustness of the linearity assumption between Tb and σ is tested in this section, as well as the spatial variation of the slope parameter β according to land-cover type. It is assumed in the SMAP mission that the parameter β relating Tb and σ is constant across each 36-km pixel, while in this study, the sensitivity parameter β is assumed constant across each 9-km pixel and estimated using the nine-day time series of Tb and σ at 9-km resolution. In terms of linearity between Tb and σ for different pols, it has been previously found that σ at vv-pol had the best correlation with Tb at h-pol and v-pol at 36-km resolution [16]. This was confirmed in this study by using Tb and σ at 9-km resolution, with respectively σ at hh-pol having a 0.1 lower correlation coefficient (R) and σ at hv-pol having a 0.25 lower R than σ at vv-pol. Therefore, in accordance with the SMAP Algorithm Theoretical Basis Document [20] and Das *et al.* [14], the σ at vv-pol was chosen to downscale Tb in this study.

TABLE I
Estimation of β (in Kelvins per Decibel) Using a Nine-Day Time Series of Tb at H-Pol and V-Pol and σ_{VV} for the Four Different Land Covers. Also Shown Is the Correlation Coefficient (R). The β for Each Land Cover Was Calculated by Merging All the Subareas With the Same Land-Cover Type

		Crops	Grass	Mixed crops and grass	Wetland
h-pol	β	-5.2	-3.0	-4.2	-11.4
	R	0.79	0.42	0.57	0.74
v-pol	β	-4.4	-2.3	-3.0	-8.6
	R	0.74	0.45	0.51	0.73

The parameter β and associated correlation coefficients between Tb and σ for the different land-cover types are presented in Table I. The β (in kelvins per decibel) for each land-cover type was calculated by merging all subareas with the same land cover. The β_h was estimated from Tb_h and σ_{vv}, while β_v was estimated from Tb_v and σ_{vv}. It is noted from Table I that the sensitivity of Tb to σ was higher in the wetland than other land-cover types, likely due to the higher scattering properties of the water body contained in the wetland. These β values, ranging from -8.6 to -2.3 at v-pol and -11.4 to -3.0 at h-pol according to land-cover type, can be compared to the β value at 36-km resolution that was estimated around -2.2 at v-pol and -3.4 at h-pol from Wu *et al.* [16]. According to these results, the assumption of a constant β within an entire SMAP 36-km pixel may be a limitation when applying the downscaling algorithm to SMAP data because of the heterogeneity across SMAP-sized pixels. For example, the different vegetation types, vegetation water content, surface roughness, etc., which impose a different sensitivity of Tb to σ, are all considered to have the same sensitivity (β) across each coarse resolution pixel.

An important consideration in estimating β is the tradeoff between robustness of the regression due to the number of data points used in the estimation and the impact of seasonality due to the length of the data window that is used. It is expected that using more data would attribute to a more accurate linear regression, but the two–three day repeat would result in a longer window that could also introduce error due to the change of land-cover condition. The value of β varies according to different seasons, as shown by Wu *et al.* [21]. Consequently, a temporal moving-window period was adopted by Das *et al.* [14] over which vegetation phenology and surface characteristics can be considered constant. In this letter, data over a three-week period were used for deriving a relatively high-fidelity algorithm parameter. While the possibility of a temporal change in β due to changes of land-cover conditions is acknowledged, this length was found to give the best results and is consistent with that used in other studies.

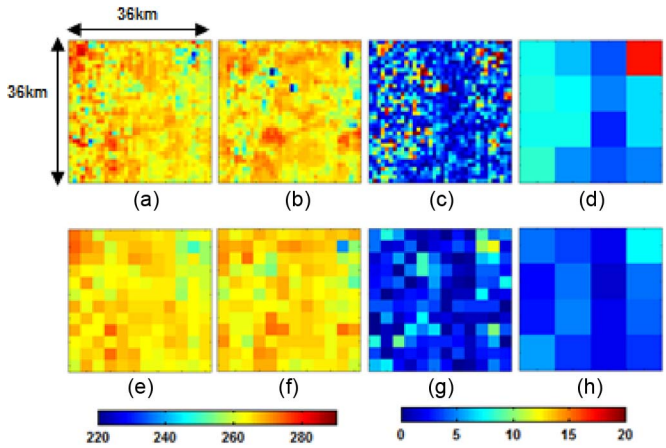

Fig. 2. Example of downscaling results on day 9 (September 23, 2011). (a) Downscaled Tb at v-pol, 1-km resolution. (b) PLMR-observed Tb at v-pol, 1-km resolution. (c) Absolute difference between (a) and (b). (d) RMSE of 1-km-resolution data in each 9-km pixel. (e)–(h) As for above but at 3-km resolution.

The parameter Γ used to denote the sensitivity of σ_{vv} to σ_{hv} was estimated from snapshots of σ_{vv} and σ_{hv} values at each 3-km pixel within the entire 9-km coarse scale pixel. In this letter, nine pairs of σ_{vv} and σ_{hv} in each 9-km area were used to calculate Γ for each 9-km area within the SMAPEx site and for each day of data. The range of Γ due to heterogeneity in vegetation was from 0.2 to 0.6. The average values of Γ were 0.34 ($\pm$0.06 standard deviation) for grassland, 0.43 ($\pm$0.14) for the mixed area, 0.46 ($\pm$0.26) for wetland, and 0.52 ($\pm$0.13) for the cropping area. Since radar backscatter σ_{hv} is more related to vegetation conditions than to soil moisture, the variation of σ_{hv} across the whole area can therefore reflect the heterogeneity of vegetation conditions to some extent, which can be further converted to σ_{vv} through the sensitivity Γ and thus reduce the influence of vegetation on the PLIS observations.

B. Downscaling Results

The baseline downscaling algorithm was applied to the nine-day data set, and the resulting downscaled Tb at both 1- and 3-km resolutions across the nine days compared with the reference Tb from PLMR at the same resolutions. Fig. 2 shows an example of downscaling for v-pol at different resolutions on day 9 (September 23, 2011), including the downscaled Tb, reference Tb, and their absolute difference, as well as the root-mean-square error (rmse) for each 9-km pixel. More statistics across the nine days are provided in Table II with respect to different land covers, different resolutions, and different pols. By combining the land classification from Fig. 1 with the rmse at 1- and 3-km resolutions from Table II, it was found that the grassland area had the best downscaling performance due to its relative homogeneity, while the wetland area had the largest error. However, this poor result for wetland is due to the fact that the water body has a considerable impact on the relationship between Tb and σ when not removed prior to downscaling, resulting in a poor estimation in the Tb variation across this particular 9-km pixel.

The rmse is reduced when going from 1 to 3 km, and it can therefore reasonably be expected to continue decreasing when upscaling to SMAP resolution. This is due in part to the reduced heterogeneity captured from observations at coarser spatial scale. Moreover, it is noted that downscaled results at v-pol have relatively lower rmse than those at h-pol, mainly due to the better linearity between σ_{vv} and Tb_v than that between σ_{vv} and Tb_h. However, there is an obvious reduction of rmse at both pols when aggregating to larger scale, e.g., a reduction of 4 K for cropping area, 2 K for grassland, 3 K for mixed area, and 6 K for wetland when aggregating from 1- to 3-km resolution.

Regarding the downscaling performance for different land covers, it is shown that the average rmses at 3-km resolution are around 2.7 K and 2.3 K at h-pol and v-pol for the grassland, 4.3 K and 3.4 K for the cropping area, 5.6 K and 4.4 K for the mixed area, and 9 K and 8.5 K for the wetland, respectively. Since the grassland is relatively homogeneous in terms of surface and vegetation conditions, while the cropping and mixed areas have much greater variation in vegetation characteristics and surface roughness, the heterogeneity in conditions for the cropping and mixed areas has resulted in a poorer estimation of β compared to the grassland and thus influenced the downscaling accuracy. As indicated from the wetland results, the water body that covered approximately 10% of the coarse pixel that contained it had a great influence on downscaling accuracy, due to the large difference in Tb between the water body and the surrounding area, highlighting the need to clean the Tb data for water bodies prior to downscaling.

The downscaled Tb target errors are around 2.4 K for SMAP [20] and 4 K for SMOS [6]. While the results in Table II show that the downscaling performance over the grassland has fulfilled the SMAP target, results in the cropping and mixed areas are around 2 K higher than the SMAP target. This implies that, while the SMAP baseline downscaling approach should perform adequately within relatively homogeneous environments, it is unlikely to meet the target accuracy in areas with varied land surface conditions. In order to assess the effect of irrigated fields within the cropping areas, irrigated farms were additionally removed prior to aggregation and downscaling, with improvements in rmse of $\sim$1.2 K at 1-km resolution and 0.4 K at 3-km resolution over the previous results. By combining different land-cover types, the downscaled Tb across the entire 36 km $\times$ 36 km area had overall rmses of around 7.2 K at h-pol and 6.1 K at v-pol at 1-km resolution, and 3.8 K at h-pol and 3.1 K at v-pol at 3-km resolution. In comparison with the results at the same resolution levels from the study by Wu *et al.* [16], the results here showed improvements of around 0.8 K at 1-km resolution and 1.5 K at 3-km resolution, indicating that a spatially variable β across SMAP pixels may have the potential to retrieve more accurate downscaling results than using a single value of β across the entire area.

V. Conclusion

The objective of this study was to test the feasibility of the proposed baseline downscaling approach proposed for the SMAP mission for a range of land surface conditions, using airborne active and passive data collected during the SMAPEx

TABLE II
RMSE (IN KELVINS) OF DOWNSCALED Tb WITH RESPECT TO DIFFERENT LAND COVERS (C = CROPS; G = GRASSLAND; M = MIXED AREA; W = WETLAND), AT DIFFERENT POLS (H-POL OR V-POL) AND RESOLUTIONS (1 AND 3 km) ACROSS NINE DAYS (D1–D9 OF SMAPEX-3)

	D1		D2		D3		D4		D5		D6		D7		D8		D9		Ave.	
	h	*v*	*h*	*v*	*h*	*v*	*h*	*v*	*h*	*v*	*h*	*v*	*h*	*v*	*h*	*v*	*h*	*v*	*h*	*v*
C_1km	8.2	7.6	8.3	7.3	8.5	7.8	9.2	7.9	8.1	7.1	8.2	7.0	7.5	6.1	8.3	6.1	8.0	5.7	8.2	6.9
G_1km	5.6	5.2	4.8	4	5.6	4.7	5.3	4.7	4.6	3.9	4.6	4.0	4.2	3.6	4.2	3.6	4.5	3.9	4.8	4.1
M_1km	9.7	7.4	9.1	7.0	8.7	7.8	9.3	8.3	8.9	6.9	7.6	6.6	8.5	6.7	7.9	6.1	7.9	6.0	8.6	6.9
W_1km	16.7	15.7	16.0	15.2	15.2	14.1	15.1	14.7	16.0	15.3	16.2	14	16.2	14.6	15.6	15.1	16	14.7	15.8	14.8
C_3km	5.7	4.5	4.6	3.6	5.8	4.8	4.8	3.7	4.4	3.7	3.1	2.3	3.3	2.8	3.5	3.0	3.7	3.0	4.3	3.4
G_3km	3.6	3.0	2.8	2.2	3.3	2.5	2.9	2.7	2.5	2.3	2.6	2.3	2.4	2.0	2.1	1.9	2.3	2.0	2.7	2.3
M_3km	6.8	5.4	6.7	5.4	5.1	4.0	6.9	5.5	5.6	4.4	5.4	4.1	5.2	4.1	4.6	3.5	4.7	3.6	5.6	4.4
W_3km	10.6	9.9	9.6	9.1	9.5	8.7	8.8	8.7	8.8	8.9	10.1	8.1	9.3	8.8	9.5	9	5.6	5.1	9	8.5

field campaign in Australia. Results indicated that application of the downscaling algorithm to grassland areas was able to meet the 2.4-K target error for SMAP downscaled Tb. However, other land-cover types such as crops and mixed land use (e.g., crops and grassland) had an error of 2 K higher than the target, due to the more complicated surface conditions. It is shown that the accuracy of the downscaling approach is primarily determined by the vegetation characteristics across the entire study area, as well as the sensitivity of brightness temperature to radar backscatter as imposed by the the parameter β. Moreover, comparing these results with those by Wu *et al.* [16] suggests that a spatially distributed β may result in a better downscaling accuracy than using the assumption of single value of β across the entire SMAP pixels. For the SMAP mission, estimation of β at finer resolution, e.g., 9 km, can possibly be obtained from its relationship with vegetation characteristics, e.g., through the Radar Vegetation Index from fine-resolution radar observations, thus providing the opportunity to retrieve downscaled Tb with higher accuracy.

ACKNOWLEDGMENT

The SMAPEx field campaigns have been funded by the Australian Research Council Discovery (DP0984586) and Infrastructure (LE0453434 and LE0882509) grants. The authors acknowledge the collaboration of scientists from throughout Australia and around the world, which provided significant contribution to the campaign's design and execution. Furthermore, the authors would like to particularly acknowledge Dr. M. Tanase for his crucial contribution to the calibration of the PLIS radar. The authors also acknowledge the scholarship awarded by Monash University to X. Wu in support of this research.

REFERENCES

[1] W. Wagner *et al.*, "Evaluation of the agreement between the first global remotely sensed soil moisture data with model and precipitation data," *J. Geophys. Res. Atmos.*, vol. 108, no. D19, pp. 4611–4619, Oct. 2003.

[2] A. Loew, T. Holmes, and R. de Jeu, "The European heat wave 2003: Early indicators from multisensoral microwave remote sensing?" *J. Geophys. Res. Atmos.*, vol. 114, no. D5, pp. D05103-1–D05103-14, Mar. 2009.

[3] L. Brocca *et al.*, "Improving runoff prediction through the assimilation of the ASCAT soil moisture product," *Hydrol. Earth Syst. Sci.*, vol. 14, no. 10, pp. 1881–1893, Oct. 2010.

[4] D. G. Miralles *et al.*, "Global land-surface evaporation estimated from satellite-based observations," *Hydrol. Earth Syst. Sci.*, vol. 15, no. 2, pp. 453–469, Feb. 2011.

[5] T. J. Jackson, A. Y. Hsu, and P. E. O'Neill, "Surface soil moisture retrieval and mapping using high-frequency microwave satellite observations in the southern great plains," *J. Hydrometeorol.*, vol. 3, no. 6, pp. 688–699, Dec. 2002.

[6] Y. H. Kerr *et al.*, "The SMOS mission: New tool for monitoring key elements of the global water cycle," *Proc. IEEE*, vol. 98, no. 5, pp. 666–687, May 2010.

[7] Y. Kerr, "Soil moisture from space: Where are we?" *Hydrogeol. J.*, vol. 15, no. 1, pp. 117–120, Sep. 2006.

[8] J. D. Albertson and M. B. Parlange, "Natural integration of scalar fluxes from complex terrain," *Adv. Water Resour.*, vol. 23, no. 3, pp. 239–252, Nov. 1999.

[9] C. P. Weaver and R. Avissar, "Atmospheric disturbances caused by human modification of the landscape," *Bull. Amer. Meteorol. Soc.*, vol. 82, no. 2, pp. 269–281, Feb. 2001.

[10] D. Entekhabi *et al.*, "The Soil Moisture Active Passive (SMAP) mission," *Proc. IEEE*, vol. 98, no. 5, pp. 704–716, May 2010.

[11] X. Zhan, P. R. Houser, J. P. Walker, and W. T. Crow, "A method for retrieving high-resolution surface soil moisture from hydros L-band radiometer and radar observation," *IEEE Trans. Geosci. Remote Sens.*, vol. 44, no. 6, pp. 1534–1544, Jun. 2006.

[12] M. Piles, D. Entekhabi, and A. Camps, "A change detection algorithm for retrieving high-resolution soil moisture from SMAP radar and radiometer observations," *IEEE Trans. Geosci. Remote Sens.*, vol. 47, no. 12, pp. 4125–4131, Dec. 2009.

[13] U. Narayan, V. Lakshmi, and T. J. Jackson, "High-resolution change estimation of soil moisture using L-band radiometer and radar observations made during the SMEX02 experiments," *IEEE Trans. Geosci. Remote Sens.*, vol. 44, no. 6, pp. 1545–1554, Jun. 2006.

[14] N. N. Das *et al.*, "Tests of the SMAP combined radar and radiometer algorithm using airborne field campaign observations and simulated data," *IEEE Trans. Geosci. Remote Sens.*, vol. 52, no. 4, pp. 2018–2028, Apr. 2014.

[15] N. N. Das, D. Entekhabi, and E. G. Njoku, "An algorithm for merging SMAP radiometer and radar data for high-resolution soil-moisture retrieval," *IEEE Trans. Geosci. Remote Sens.*, vol. 49, no. 5, pp. 1504–1512, May 2011.

[16] X. Wu, J. P. Walker, N. N. Das, R. Panciera, and C. Rüdiger, "Evaluation of the SMAP brightness temperature downscaling algorithm using active-passive microwave observations," *Remote Sens. Environ.*, to be published.

[17] R. Panciera *et al.*, "The Soil Moisture Active Passive Experiments (SMAPEx): Toward soil moisture retrieval from the SMAP mission," *IEEE Trans. Geosci. Remote Sens.*, vol. 52, no. 1, pp. 490–507, Jan. 2014.

[18] X. Wu, J. P. Walker, C. Rüdiger, R. Panciera, and D. A. Gray, "Simulation of the SMAP data stream from SMAPEx field campaigns in Australia," *IEEE Trans. Geosci. Remote Sens.*, vol. 53, no. 4, pp. 1921–1934, Apr. 2015.

[19] N. Ye, J. P. Walker, and C. Rüdiger, "A cumulative distribution function method for normalising multi-angle microwave observations," *IEEE Trans. Geosci. Remote Sens.*, submitted for publication.

[20] D. Entekhabi, N. N. Das, E. G. Njoku *et al.*, Algorithm Theoretical Basis Document: L2 & L3 Radar/Radiometer Soil Moisture (Active/Passive) Data Products, Initial Release, v. 1. [Online]. Available: http://smap.jpl.nasa.gov/files/smap2/L2&3_SM_AP_InitRel_v11.pdf

[21] X. Wu *et al.*, "Towards medium-resolution brightness temperature retrieval from active and passive microwave," in *Proc. MODSIM*, 2011, pp. 2023–2029.